$$-V_{ehijpl}=\frac{j\frac{2\pi}{\lambda}}{\sqrt{\gamma_{hpl}^{(1)}\gamma_{eij}^{(2)}}}\int_{F_1}\left(-\vec{e}_{hpl}^{(1)}\right)\left(\vec{e}_{eij}^{(2)}\right)dx\,dy \tag{A3}$$

$$V_{eeijpl}=\sqrt{\frac{\gamma_{epl}^{(1)}}{\gamma_{eij}^{(2)}}}\int_{F_1}\left(\vec{e}_{epl}^{(1)}\right)\left(\vec{e}_{eij}^{(2)}\right)dx\,dy \tag{A4}$$

where F_1 = area of waveguide 1 (see Fig. 1(b)). The vectors $\vec{e}$ denote

$$\vec{e}_{hpl}^{(1)}=\vec{e}_z\times\nabla_{xy}T_{hpl}^{(1)} \tag{A5}$$

$$\vec{e}_{epl}^{(1)}=\nabla_{xy}T_{epl}^{(1)} \tag{A6}$$

$$\vec{e}_{hij}^{(2)}=\vec{e}_z\times\nabla_{xy}T_{hij}^{(2)} \tag{A7}$$

$$\vec{e}_{eij}^{(2)}=\nabla_{xy}T_{eij}^{(2)}. \tag{A8}$$

References

[1] G. Matthaei, L. Young, and E. M. T. Jones, *Microwave Filters, Impedance-Matching Networks, and Coupling Structures*. New York: McGraw-Hill, 1964.

[2] S. B. Cohn, "Optimum design of stepped transmission-line transformers," *IRE Trans. Microwave Theory Tech.*, vol. MTT-3, pp. 16–21, Apr 1955.

[3] H. J. Riblet, "General synthesis of quarter-wave impedance transformers," *IRE Trans. Microwave Theory Tech.*, vol. MTT-5, pp. 36–43, 1957.

[4] H. Patzelt, and F. Arndt, "Double-plane steps in rectangular waveguides and their application for transformers, irises, and filters," *IEEE Trans. Microwave Theory Tech.*, vol. MTT-30, pp. 771–776, May 1982.

[5] R. Safavi-Naini and R. H. MacPhie, "Scattering at rectangular-to-rectangular waveguide junctions," *IEEE Trans. Microwave Theory Tech.*, vol. MTT-33, pp. 2060–2063, Nov. 1982.

[6] Y. C. Shih and K. G. Gray, "Convergence of numerical solutions of step-type waveguide discontinuity problems by modal analysis," in *1983 MTT-S Int. Microwave Symp. Dig.* (Boston), pp. 233–235.

[7] H. Patzelt and F. Arndt, "Mehrstufige inhomogene Rechteck-Hohlleitertransformatoren," *Frequenz*, vol. 32, pp. 233–239, Aug. 1978.

[8] R. E. Collin, *Field Theory of Guided Waves*. New York: McGraw-Hill, 1960.

[9] M. S. Navarro, T. E. Rozzi, and Y. T. Lo, "Propagation in a rectangular waveguide periodically loaded with resonant irises," *IEEE Trans. Microwave Theory Tech.*, vol. MTT-28, pp. 857–865, Aug. 1980.

[10] T. Rozzi, "A new approach to the network modeling of capacitive irises and steps in waveguide," *Int. J. Circuit Theory Appl.*, vol. 3, pp. 339–354, Dec. 1975.

[11] H. Schmiedel, "Anwendung der Evolutionsoptimlerung bei Milrowellenschaltungen," *Frequenz*, vol. 35, pp. 306–310, Nov. 1980.

Analysis of Finline with Finite Metallization Thickness

TOSHIHIDE KITAZAWA AND RAJ MITTRA, FELLOW, IEEE

***Abstract*—In this paper, we present a method for analyzing finline structures with finite metallization thickness. The method is based on a hybrid mode formulation but it by-passes the lengthy process of formulating the determinantal equation for the unknown propagation constant. Some numerical results are presented to show the effect of the metallization thickness for unilateral and bilateral finlines.**

Manuscript received October 6, 1983; revised June 11, 1984. This work was supported in part by DAAG29-82-K-0084 and JSEP N000-1479C-0424.

The authors are with the Electrical Engineering Department, University of Illinois, Urbana, IL. T. Kitazawa is on leave from the Kitami Institute of Technology, Kitami, Japan.

I. Introduction

Finline structures have received considerable attention because of their usefulness as millimeter-wave integrated-circuit components. Recently, two efficient numerical methods for analyzing the propagation characteristics of finline structures were presented. The first of these employs the spectral-domain technique [1], [2], whereas the second utilizes network analytical methods for electromagnetic fields [3]. Both of these methods are based on the hybrid mode formulation, but they neglect the effect of the metallization thickness, which increases with higher operating frequencies and narrower gaps in the metallization. An eigenvalue equation for a unilateral finline with a finite metallization thickness has been previously derived [4] using the hybrid mode formulation, but only approximate results based on the TE-approximation have been presented in the above paper. In this paper, we discuss an efficient hybrid mode formulation for the finite metallization problem and derive the solution to the problem without resorting to the TE-approximation. Although the method is an extension of the treatment in [3], [5], and [6], it derives Green's functions using the conventional circuit theory rather than by directly solving the differential equations with boundary conditions.

II. The Network Formulation of the Problem

The unilateral finline shown in Fig. 1 is used to illustrate the formulation procedure, but the method itself is quite general.

As a first step, we express the transverse (to z) fields in each region by the following spectral representation:

$$\left.\begin{matrix}\bar{E}_t^{(i)}(x,y,z)\\ \bar{H}_t^{(i)}(x,y,z)\end{matrix}\right\}=\sum_{l=1}^{2}\sum_{n=0}^{\infty}\left\{\begin{matrix}V_{ln}^{(i)}(z)\bar{f}_{ln}^{(i)}(x)\\ I_{ln}^{(i)}(z)\bar{g}_{ln}^{(i)}(x)\end{matrix}\right\}e^{-j\beta_0 y},\qquad i=1,2,3,4 \tag{1}$$

where the vector mode functions $\bar{f}_{ln}^{(i)}$ and $\bar{g}_{ln}^{(i)}$ in each region are given as

A) region (1), (3), and (4)

$$\bar{f}_{1n}^{(i)}=\frac{-1}{K_A}\sqrt{\frac{\eta_n}{2A}}\left\{\bar{x}_0\alpha_A\cos(\alpha_A x)-\bar{y}_0 j\beta_0\sin(\alpha_A x)\right\}$$

$$\bar{f}_{2n}^{(i)}=\frac{1}{K_A}\sqrt{\frac{\eta_n}{2A}}\left\{\bar{x}_0 j\beta_0\cos(\alpha_A x)-\bar{y}_0\alpha_A\sin(\alpha_A x)\right\}$$

$$\bar{g}_{ln}^{(i)}=\bar{z}_0\times\bar{f}_{ln}^{(i)}\qquad(l=1,2)$$

$$\alpha_A=\frac{n\pi}{A},\quad K_A=\sqrt{\alpha_A^2+\beta_0^2}$$

$$\eta_n=\begin{cases}1\ (n=0)\\ 2\ (n\neq 0)\end{cases}. \tag{2}$$

B) region (2)

$$\bar{f}_{1n}^{(2)}=\frac{-1}{K_W}\sqrt{\frac{\eta_n}{2W}}\left\{\bar{x}_0\alpha_W\cos(\alpha_W x)-\bar{y}_0 j\beta_0\sin(\alpha_W x)\right\}$$

$$\bar{f}_{2n}^{(2)}=\frac{1}{K_W}\sqrt{\frac{\eta_n}{2W}}\left\{\bar{x}_0 j\beta_0\cos(\alpha_W x)-\bar{y}_0\alpha_W\sin(\alpha_W x)\right\}$$

$$\bar{g}_{ln}^{(2)}=\bar{z}_0\times\bar{f}_{ln}^{(2)}\qquad(l=1,2),\ \alpha_W=\frac{n\pi}{W},\ K_W=\sqrt{\alpha_W^2+\beta_0^2} \tag{3}$$

where β_0 is the propagation constant, and $\bar{x}_0$, $\bar{y}_0$, and $\bar{z}_0$ are the x-, y-, and z-directed unit vectors, respectively. It should be noted that the vector mode functions $\bar{f}_{\ln}^{(i)}$, $\bar{g}_{\ln}^{(i)}$ satisfy the

0018-9480/84/1100-1484$01.00 ©1984 IEEE

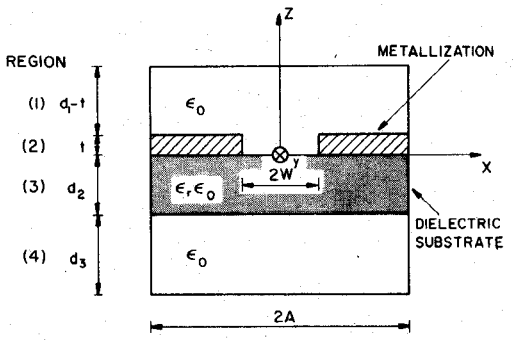

Fig. 1. Unilateral finline.

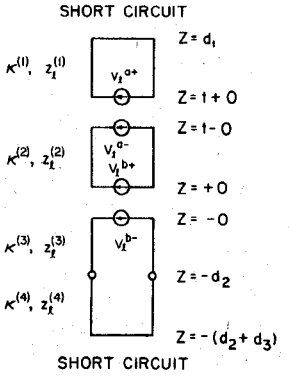

Fig. 2. Equivalent circuits for transverse section of finline.

boundary conditions at $x = \pm W$ and $\pm A$ and the orthonormal properties.

Substituting (1) into Maxwell's field equations, we obtain the differential equations for the modal voltages and currents

$$-\frac{d}{dz}V_{ln}^{(i)} = j\kappa^{(i)}z_l^{(i)}I_{ln}^{(i)}$$
$$-\frac{d}{dz}I_{ln}^{(i)} = j\kappa^{(i)}y_l^{(i)}V_{ln}^{(i)} \tag{4}$$

where

$$\kappa^{(i)} = \sqrt{\omega^2\epsilon^{(i)}\mu_0 - K^{(i)2}}$$

$$\epsilon^{(i)} = \begin{cases} \epsilon_r\epsilon_0 & \text{(region (3))} \\ \epsilon_0 & \text{(otherwise)} \end{cases} \qquad K^{(i)} = \begin{cases} K_W & \text{(region (2))} \\ K_A & \text{(otherwise)} \end{cases}$$

$$z_1^{(i)} = \frac{\kappa^{(i)}}{\omega\epsilon^{(i)}}, \qquad z_2^{(i)} = \frac{\omega\mu_0}{\kappa^{(i)}}$$

$$y_l^{(i)} = \frac{1}{z_l^{(i)}} \qquad (l=1,2). \tag{5}$$

Equivalent circuits in the z-direction can be derived by considering the differential equations (4) together with the associated boundary conditions (Fig. 2). The equivalent voltage sources $\mathcal{V}_l^{a\pm}, \mathcal{V}_l^{b\pm}$ shown in this figure are given by

$$\left.\begin{matrix}\mathcal{V}_l^{a+} \\ \mathcal{V}_l^{a-}\end{matrix}\right\} = \int_{-W}^{W} \left\{\begin{matrix}\bar{f}_{ln}^{(1)*}(x') \\ \bar{f}_{ln}^{(2)*}(x')\end{matrix}\right\} \cdot \bar{e}_a(x')\,dx' \tag{6a}$$

$$\left.\begin{matrix}\mathcal{V}_l^{b+} \\ \mathcal{V}_l^{b-}\end{matrix}\right\} = \int_{-W}^{W} \left\{\begin{matrix}\bar{f}_{ln}^{(2)*}(x') \\ \bar{f}_{ln}^{(3)*}(x')\end{matrix}\right\} \cdot \bar{e}_b(x')\,dx' \tag{6b}$$

and where $\bar{e}_a$ and $\bar{e}_b$ are the transverse electric fields at $z = t$ and $z = 0$, respectively

$$\bar{e}_a = \bar{x}_0 e_{ax} + \bar{y}_0 e_{ay}. \tag{7}$$

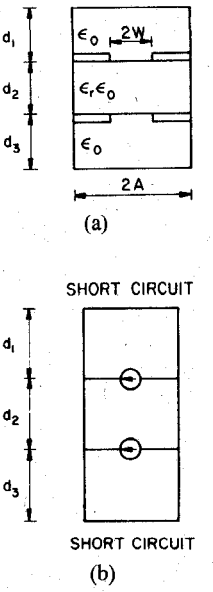

Fig. 3. Bilateral finline (metallization thickness is neglected in this figure).

The modal voltages $V_{ln}^{(i)}$ and currents $I_{ln}^{(i)}$ in each region can be obtained by using conventional circuit theory. Electromagnetic fields in each region can then be derived by substituting $V_{ln}^{(i)}$ and $I_{ln}^{(i)}$ into (1). Finally, the application of the continuities of magnetic fields results in the following set of equations for the unknown electric fields $\bar{e}_a$ and $\bar{e}_b$ at $z = t$ and $z = 0$, and for the unknown propagation constant β_0:

$$\sum_{l=1}^{2}\sum_{n=0}^{\infty}\int_{-W}^{W} Y_l^{(1)}(t+0|t)\,\bar{g}_{ln}^{(1)}(x)\bar{f}_{ln}^{(1)*}(x')\cdot\bar{e}_a(x')\,dx'$$
$$= \sum_{l=1}^{2}\sum_{n=0}^{\infty}\int_{-W}^{W}\Big\{ Y_l^{(2)}(t-0|t)\,\bar{g}_{ln}^{(2)}(x)\bar{f}_{ln}^{(2)*}(x')\cdot\bar{e}_a(x')$$
$$+ Y_l^{(2)}(t-0|0)\,\bar{g}_{ln}^{(2)}(x)\bar{f}_{ln}^{(2)*}(x')\cdot\bar{e}_b(x')\Big\}\,dx' \tag{8a}$$

$$\sum_{l=1}^{2}\sum_{n=0}^{\infty}\int_{-W}^{W}\Big\{ Y_l^{(2)}(+0|t)\,\bar{g}_{ln}^{(2)}(x)\bar{f}_{ln}^{(2)*}(x')\cdot\bar{e}_a(x')$$
$$+ Y_l^{(2)}(+0|0)\,\bar{g}_{ln}^{(2)}(x)\bar{f}_{ln}^{(2)*}(x')\cdot\bar{e}_b(x')\Big\}\,dx'$$
$$= \sum_{l=1}^{2}\sum_{n=0}^{\infty}\int_{-W}^{W} Y_l^{(3)}(-0|0)\,\bar{g}_{ln}^{(3)}(x)\bar{f}_{ln}^{(3)*}(x')\cdot\bar{e}_b(x')\,dx' \tag{8b}$$

where $Y_l^{(i)}(z|z')$ are the Green's functions which relate the modal currents $I_l^{(i)}(z)$ to the voltage source in each of the three regions. The set of equations (8) is rigorous. Numerical solution of the equations is discussed in the next section.

The equivalent circuit concept, which is used to derive the Green's functions, is similar to that introduced in [2], but is extended here to treat the geometry with a finite metallization thickness. We remark here that the method itself is quite general and can be applied equally well to other finline structures. For example, Fig. 3(b) shows the equivalent circuits for the bilateral finline whose geometry is given in Fig. 3(a).

III. Numerical Computations

The numerical procedure for solving (8) is analogous to that used in [3], [5], and [6]; therefore, only a summary of the steps will be given below.

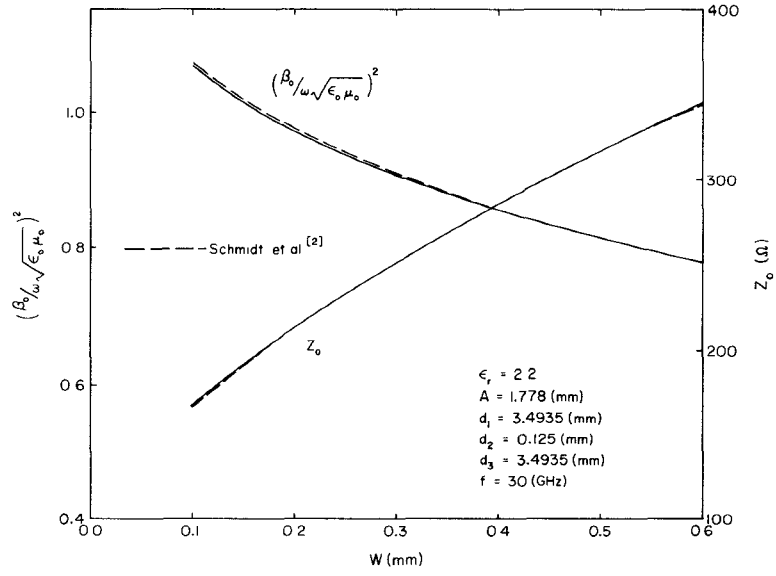

Fig. 4. The comparison of this method with other method (the unilateral finline with zero metallization thickness).

The first step is to expand the unknown electric fields $\bar{e}_a$ and $\bar{e}_b$ at $z=t$ and 0, in terms of an appropriate set of basis

$$\left.\begin{matrix} e_{xa}(x) \\ e_{xb}(x) \end{matrix}\right\} = \sum_{k=1}^{2N_x} \left\{\begin{matrix} a_{xk} \\ b_{xk} \end{matrix}\right\} f_{xk}(x)$$

$$\left.\begin{matrix} e_{ya}(x) \\ e_{yb}(x) \end{matrix}\right\} = j \sum_{k=1}^{2N_y} \left\{\begin{matrix} a_{yk} \\ b_{yk} \end{matrix}\right\} f_{yk}(x) \qquad (9)$$

where a_y^{xk} and b_y^{xk} are the unknown coefficients. The second step is to apply the Galerkin's procedure to (8), which results in the determinantal equation for the propagation constant β_0. Finally, the determinantal equation is solved for β_0 in the finline structure. Accurate solutions can be obtained with only a small number of basis functions, if these functions incorporate the edge effect. The following basis functions were used for the numerical results presented in this paper:

$$f_{x1}(x) = 1,$$

$$f_{xk}(x) = \frac{T_{k-2}\left(\frac{x}{W}\right)}{\sqrt{1-\left(\frac{x}{W}\right)^2}}, \qquad k = 2,3,\cdots$$

$$f_{yk}(x) = U_k\left(\frac{x}{W}\right), \qquad k = 1,2,3,\cdots \qquad (10)$$

where $T_k(y)$ and $U_k(y)$ are the Chebyshev's polynomials of the first and second kind, respectively.

Preliminary computations show that $N_x = N_y = 2$ in (9) is sufficient for deriving accurate results for finite metallization thickness, just as in the case of zero metallization thickness [3].

The numerical results obtained by this method are plotted in Fig. 4 together with the published data [4] for the unilateral finline with zero metallization thickness ($t=0$) and close agreement between the two sets of results is seen for a wide range of slot widths. The effective dielectric constant and the characteristic impedance Z_0 are defined as

$$Z_0 = \frac{\left(\beta_0/\omega\sqrt{\epsilon_0\mu_0}\right)^2 V_0^2}{2P_{av}} \qquad (11)$$

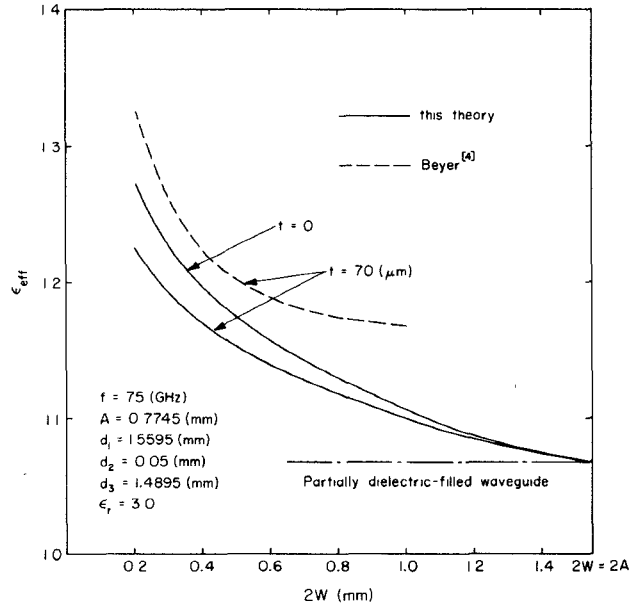

Fig. 5. Slot width dependence of the effective permittivity for unilateral finline.

where V_0 is the voltage between the fins and P_{av} is the average power flow along the y-direction.

Fig. 5 shows the slot-width dependence of the effective permittivity ϵ_{eff} for the unilateral finline with a finite metallization thickness ($t = 70$ μm). The effective permittivity ϵ_{eff} is defined by [4]

$$\lambda_g = \lambda_0 \left\{ \epsilon_{\text{eff}} - \left(\frac{\lambda_0}{\lambda_c}\right)^2 \right\}^{-1/2} \qquad (12)$$

where λ_g is the wavelength in finline, λ_0 is the free-space wavelength, and λ_c is the cutoff wavelength of a ridged waveguide of identical dimensions. The values for the case with zero metallization thickness ($t=0$) are presented for comparison. It is seen that the effect of the metallization thickness becomes smaller as the slot width becomes larger. We also note that the results for the limiting case of $W=A$ converge to those for the partially

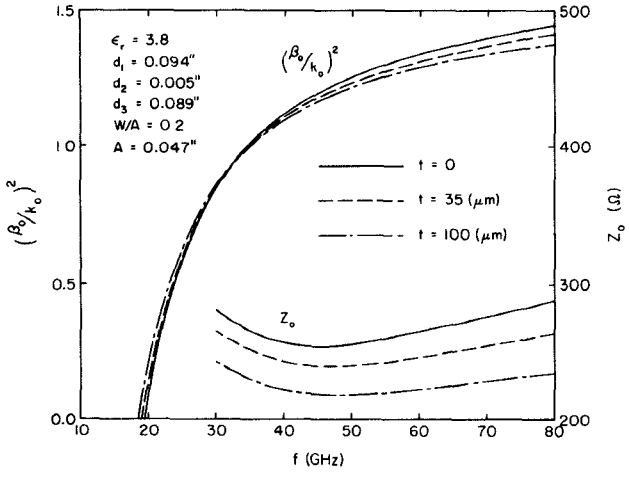

Fig. 6. Propagation characteristics of unilateral finline.

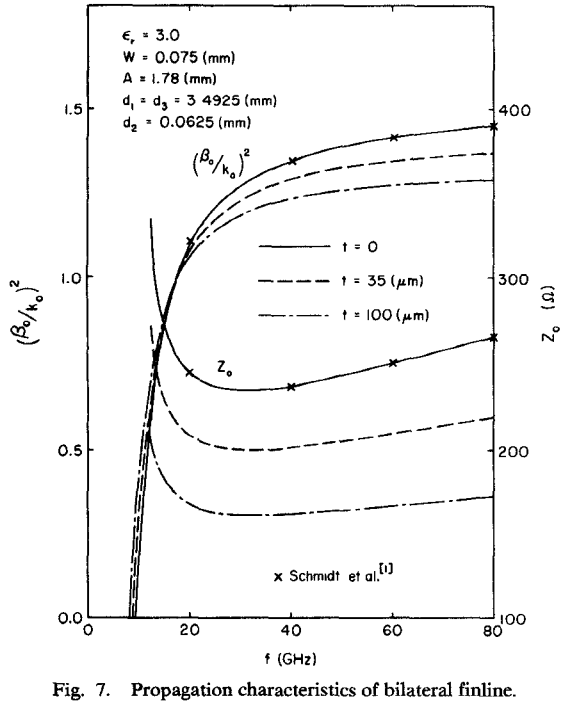

Fig. 7. Propagation characteristics of bilateral finline.

filled dielectric waveguide both for the finite and zero thickness of the metallization. However, when our results are compared with the published data by Beyer [4], some discrepancies are noted. The values obtained by Beyer are larger than those for the case of infinitely thin metallization ($t = 0$), and they do not appear to converge to a correct limiting value as W approaches A, as they should.

Fig. 6 shows the frequency dependence of the effect of the metallization thickness on the effective dielectric constant, and on the characteristic impedance in a unilateral finline. The finite thickness reduces the propagation constant in the higher frequency range as it does in the open slot line [5], because in these frequency ranges the fields are concentrated near the gap in the finline and it acts similar to an open slot line. In contrast, a finline behaves as a ridged waveguide near the cutoff frequency, and consequently, the thicker its diaphragm, the lower its cutoff frequency [7].

Fig. 7 shows the effect of the metallization thickness of a bilateral finline. The results for the limiting case of $t = 0$, i.e., zero metallization thickness, are compared with those published by Schmidt and Itoh [1], and the agreement is quite good.

IV. Conclusions

In this paper, the hybrid mode formulation was used to analyze finline structures with finite metallization thicknesses. This formulation used in conjunction with the equivalent circuit analysis is considerably simpler than the conventional Green's function approach. This method itself is quite general and can be applied to different types of finline structures by a simple modification of equivalent circuits which can be obtained easily.

Numerical results are presented to show the effects of finite metallization thickness on the propagation characteristics of unilateral and bilateral finline structures.

References

[1] L. P. Schmidt and T. Itoh, "Spectral domain analysis of dominant and higher order modes in fin-lines," *IEEE Trans. Microwave Theory Tech.*, vol. MTT-28, pp. 981–985, Sept. 1980.

[2] L. P. Schmidt, T. Itoh, and H. Hofman, "Characteristics of unilateral fin-line structures with arbitrary located slots," *IEEE Trans. Microwave Theory Tech.*, vol. MTT-29, pp. 352–355, Apr. 1981.

[3] Y. Hayashi, E. Farr, S. Wilson, and R. Mittra, "Analysis of dominant and higher-order modes in unilateral finlines," *Arch. Elek. Übertragung.*, vol. 37, no. 3/4, pp. 117–122, Mar.–Apr. 1983.

[4] A. Beyer, "Analysis of characteristics of an earthed finline," *IEEE Trans. Microwave Theory Tech.*, vol. MTT-29, pp. 676–680, July 1981.

[5] T. Kitazawa, Y. Hayashi, and M. Suzuki, "Analysis of the dispersion characteristic of slot line with thick metal coating," *IEEE Trans. Microwave Theory Tech.*, vol. MTT-28, pp. 387–392, Apr. 1980.

[6] T. Kitazawa, Y. Hayashi, and M. Suzuki, "A coplanar waveguide with thick metal coating," *IEEE Trans. Microwave Theory Tech.*, vol. MTT-24, pp. 604–608, Sept. 1976.

[7] J. R. Pyle, "The cutoff wavelength of the TE_{10} mode in ridged rectangular waveguide of any aspect ratio," *IEEE Trans. Microwave Theory Tech.*, vol. MTT-14, pp. 175–183, Apr. 1966.

An Evanescent Mode Waveguide Bandpass Filter at *Q* Band

N. P. AKERS AND P. D. ALLAN

***Abstract*—Evanescent-mode filters have previously been restricted in frequency to *X* band or below. Here, the performance of an evanescent-mode waveguide bandpass filter with a center frequency in the 26–40-GHz band (*Q* band) is reported.**

I. Introduction

The design principles of evanescent-mode waveguide filters have been developed over a number of years by Craven, Mok, [1]–[3] and others [4], [5]. Initially, those principles were based on image parameter theory but a more refined technique was later developed which employed equivalent circuits to accurately represent the below-cutoff guide and its obstacles.

Manuscript received November 2, 1983; revised May 31, 1984.

N. P. Akers was with M.S.D.S., Ltd., Frimley, Surrey, U.K. He is now with the Department of Electrical and Electronic Engineering, Portsmouth Polytechnic, Portsmouth, Hampshire, U.K.

P. D. Allan is with M.S.D.S. Ltd., Grimley, Surrey, U.K.

0018-9480/84/1100-1487$01.00 ©1984 IEEE